Case history: A 5 km long waterborne geophysical survey along the Po river within the city of Turin (northwest Italy)

GEOPHYSICS, VOL. 82, NO. 6 (NOVEMBER-DECEMBER 2017); P. B189–B199, 13 FIGS.
10.1190/GEO2017-0071.1

DOI:10.1190/geo2017-0071.1

Case History

Case history: A 5 km long waterborne geophysical survey along the Po river within the city of Turin (northwest Italy)

Luigi Sambuelli[1], Adriano Fiorucci[1], Paolo Dabove[1], Ivan Pascal[1], Chiara Colombero[2], and Cesare Comina[2]

ABSTRACT

The geologic investigation of water-covered areas is often difficult and inefficient with only the use of traditional surveying techniques (i.e., local drilling and sampling). Waterborne geophysical surveys can offer a valuable alternative to achieve adequate data coverage in a cost-effective way. Two geophysical waterborne methods were combined in this study for the delineation of the submerged subsurface geology along a 5 km stretch of the Po river, within the urban area of Turin. The adopted methods were: continuous vertical electrical sounding (CVES) and ground-penetrating radar (GPR). Special attention was devoted to the accurate geo-referencing of both surveys for combined interpretation. GPR results provide a high-quality representation of the river bed forms, with identification of clear sand dunes in the finer alluvial sediments. CVES resistivity sections enable a deeper characterization, identifying the interface between the shallow alluvial deposits and the deeper low-resistivity marls of the Turin-Hill succession. Our work strengthens the effectiveness of waterborne surveys for geologic prospecting of water-covered and difficult-to-access areas.

INTRODUCTION

This research work is focused on the application of geophysical methods as a support to geologic and hydrogeologic investigations of shallow inland water-covered areas. Among the available geophysical techniques, the use of nonseismic methods with this aim has received growing attention in recent years. A detailed review on the topic can be found, for example, in the special issue of *Near Surface Geophysics* specifically devoted to waterborne geophysics (Butler, 2009; Sambuelli and Butler, 2009).

Among nonseismic methods, applications of ground-penetrating radar (GPR) to freshwater environments have been reported since the late 1970s (Annan and Davis, 1977). More recent case histories highlighted the potentialities and cost effectiveness of waterborne GPR for bathymetry estimation and for the characterization of bottom sediments and bed forms (Arcone et al., 2006, 2010; Lin et al., 2010; Sambuelli and Bava, 2011).

In addition, the waterborne continuous vertical electrical sounding (CVES) method has been widely applied in shallow-water areas, using different electrode configurations, with similar characterization purposes (e.g., Bradbury and Taylor, 1984; Loke and Lane, 2004; Allen and Merrick, 2007; Mitchell et al., 2008; Rucker et al., 2011; Befus et al., 2012; Colombero et al., 2014). CVES data can provide information on the electrical resistivity distribution within riverbed sediments, enabling the indirect reconstruction of the underwater geologic environment. According to previous studies, floating electrodes offer faster data acquisition and avoid the practical problems of submerged cables dragged on the river bottom. Exponentially spaced floating potential electrodes are known to provide a higher resolution with depth (Allen and Merrick, 2007). Acquired CVES data can be inverted using laterally constrained inversion (LCI) and electrical resistivity tomography (ERT) approaches.

The simultaneous acquisition of CVES and GPR data can therefore provide an effective imaging of the resistivity distribution

Manuscript received by the Editor 31 January 2017; revised manuscript received 23 June 2017; published ahead of production 07 July 2017; published online 21 August 2017.
[1]Department of Environment, Land and Infrastructure Engineering — DIATI, Politecnico di Torino, Torino, Italy. E-mail: luigi.sambuelli@polito.it; adriano.fiorucci@polito.it; paolo.dabove@polito.it; ivan.pascal@studenti.polito.it.
[2]Università degli Studi di Torino, Department of Earth Sciences — DST, Torino, Italy. E-mail: chiara.colombero@unito.it; cesare.comina@unito.it.

within the riverbed sediments and a high-resolution representation of the river bottom properties. In addition, the bathymetry obtained from GPR data can supply a valuable constraint to CVES data inversion. However, a contemporary data acquisition and interpretation require an accurate geo-referencing of both surveys if they will be used for combined interpretation.

Within this context, a 5 km long stretch of the Po river in the city of Turin (northwest Italy) was investigated combining GPR and CVES surveys. The investigated river stretch is located within the urban area of Turin, downstream and north to the confluence of the Po tributary river Sangone (Figure 1). In this context, the Po river delimits the western side of the so-called Turin Hill, on the right bank, from the Po Plain, and Turin city center, on the left bank (Figure 1). A first GPR test survey on a 300 m long stretch (included in the stretch under examination) was already performed in autumn 2005 (Sambuelli et al., 2009).

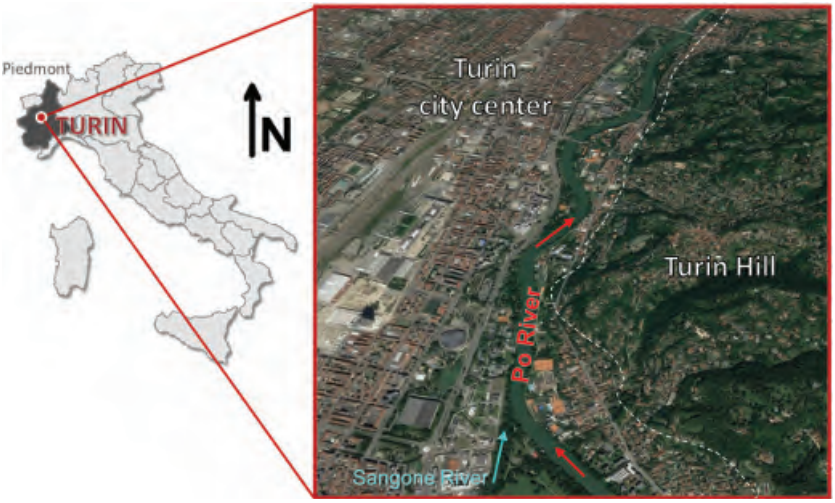

Figure 1. Geographical location of the test site.

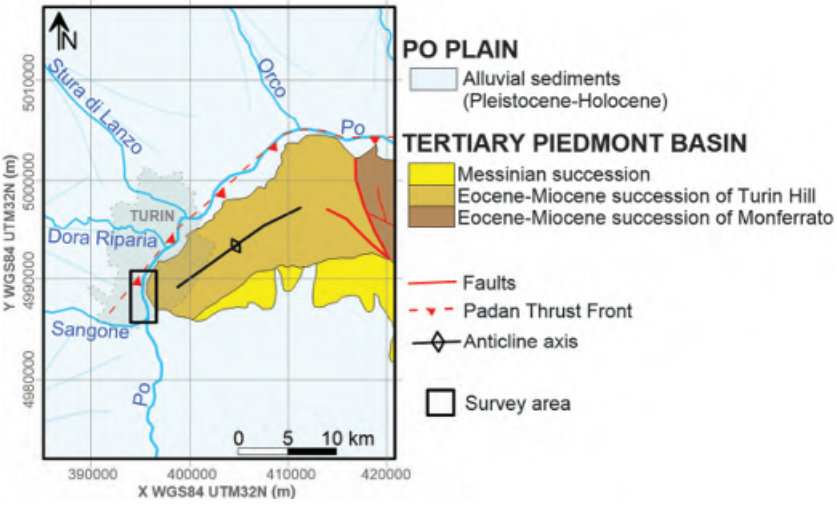

Figure 2. Structural geologic model of the Turin Hill and Po Plain in the area of Turin city center (modified from Forno and Lucchesi, 2015) with evidence of the survey area, whose detail is the area reported in Figure 3.

The main purpose of this study was the characterization of the riverbed sediments to define nature, composition, geometry, and spatial relationships of the detected water-covered bodies. Peculiar attention was devoted to the spatial reconstruction of the submerged/buried interface between the Po alluvial sediments and the Turin Hill formation, which is mainly composed of marly deposits. Position, depth, and lateral continuity of this interface are indeed crucial for hydrogeological and geotechnical reasons. First, this interface, between the coarse permeable alluvial deposits and the low-permeability marls, is of primary interest because it represents the base of the shallowest aquifers interacting with the river flow and shallow surface water. Second, this interface must be taken into account for the design of any engineering work across or below the river, due to the highly deformable nature of the marly deposits.

Available stratigraphic information (e.g., stratigraphic logs, water wells, etc.) on this interface are too sparse to allow a reliable estimate of its lateral continuity and depth. Moreover, log reports often lack in accurate descriptions to allow precise evaluation of the composition of the overlying deposits and their lateral variability. Increasing this available knowledge by means of direct investigations (e.g., increasing the number of drillings or sampling the river bottom) would be neither cost effective nor reasonably quick because an extremely high number of new exploratory drillings would be necessary. These investigations would be even more complicated in the studied context, due to the highly urbanized river banks and related problems with drilling permission and organization (i.e., space limitations). Particularly, the right bank of the river is characterized by the presence of a high-traffic road.

Therefore, waterborne geophysical surveys can offer a valuable alternative to achieve a more adequate data coverage in a cost-effective way. After the presentation of the main geologic and hydrologic features of the area, the strategies adopted for data acquisition and processing are described. Obtained results are then discussed and compared with available information and literature data.

GEOLOGIC AND HYDROGEOLOGIC BACKGROUND

In the urban area of the city of Turin, the Po river flows at the western edge of the southwest–northeast-elongated reliefs of the Turin-Hill anticline. This northwest-verging structure overthrusts onto the Po Plain along the Padan Frontal Thrust, currently buried by Quaternary fluvial sediments (Castellarin, 1994; Mosca, 2006; Festa et al., 2009). A simplified geologic model of the area is reported in Figure 2. Particularly, the reliefs to the west of the city center consist of a folded Eocene-Miocene marine succession (Bortolami et al., 1969), belonging to the shallow marginal zones of the Tertiary Piedmont Basin. This succession is identified in literature as Turin Hill,

DOI:10.1190/geo2017-0071.1

close to the city, and Monferrato, to the west. Later chaotic Messinian units (muddy deposits with gypsum and carbonate blocks), overlap the marine succession at the southern edge of the reliefs (Dela Pierre et al., 2012).

Within the Turin Hill, the most superficial formation from the Eocene-Miocene succession is the Baldissero Unit (Synthem III Langhian). This unit consists of marls with subordinated sandstones and arenaceous-conglomeratic bodies. Its outcropping area extends for several kilometers within the hill, with thicknesses varying between 50 and 350 m. Several authors (e.g., Sangiovanni, 2017) report an average permeability for this unit lower than 10^{-8} m/s.

Above this unit, different deposits belonging to synthems of San Vito (Middle Pleistocene), Cavoretto (Upper Pleistocene), and Monte dei Cappuccini (Upper Pleistocene) can be found. These synthems are suspended stream terraces stored on the north and northwest slopes of the Turin Hill, with varying thickness (between 1 and 5 m) and are covered by aeolian deposits (Forno et al., 2002; Boano et al., 2004; Forno and Lucchesi, 2005). They generally consist of sands, silts, and weathered gravels. At the foot of the northwest side of the Turin Hill, in the right bank of the Po river, the Baldissero Unit is also covered by extensive fluvial deposits (Upper Pleistocene — Holocene), related to the Po river and tributary stream flows and alluvial fans, of unknown thickness. These are composed of gravels and fresh or slightly weathered sandy gravels, locally covered by thin layers of sands and silty sands. Available data (Lollino et al., 2000) on the shallower deposits within the city of Turin report an average permeability of 10^{-3}m/s. Below this Quaternary high-permeability cover, the low-permeability marly deposits of the Turin Hill are expected to continue at depth, progressively deepening toward the northwest. The Po river is well-recognized to be a drainage bar for the water table within the city, through the most permeable shallower deposits, and no major variations are expected between the river water and the water table itself (e.g., Civita and Pizzo, 2001; Bove et al., 2005).

The deepening toward northwest of the Turin-Hill successions below the alluvial fan sediments of the Po plain is generally poorly known. Available stratigraphic data in the area come from the Regional Agency for Environmental Protection (ARPA Piemonte, 2016) and refer to previous geognostic surveys and well logs (Figure 3). They suggest a significant variability of the depth of the Baldissero Unit along the investigated stretch, from less than 10 m (S15) to more than 20 m depth (S6), with abrupt lateral variations (e.g., the interface depth diverges of approximately 10 m from S15 to S16). Moreover, the thickness and dominant grain size of the above alluvial sediments can be only extrapolated from few sparse stratigraphic descriptions. Given the high contrast in hydrogeological (porosity and permeability) and geotechnical parameters between the alluvial deposits and the underlying marly deposits, the spatial reconstruction of this interface below the city center is of peculiar practical interest and is the main object of the surveys.

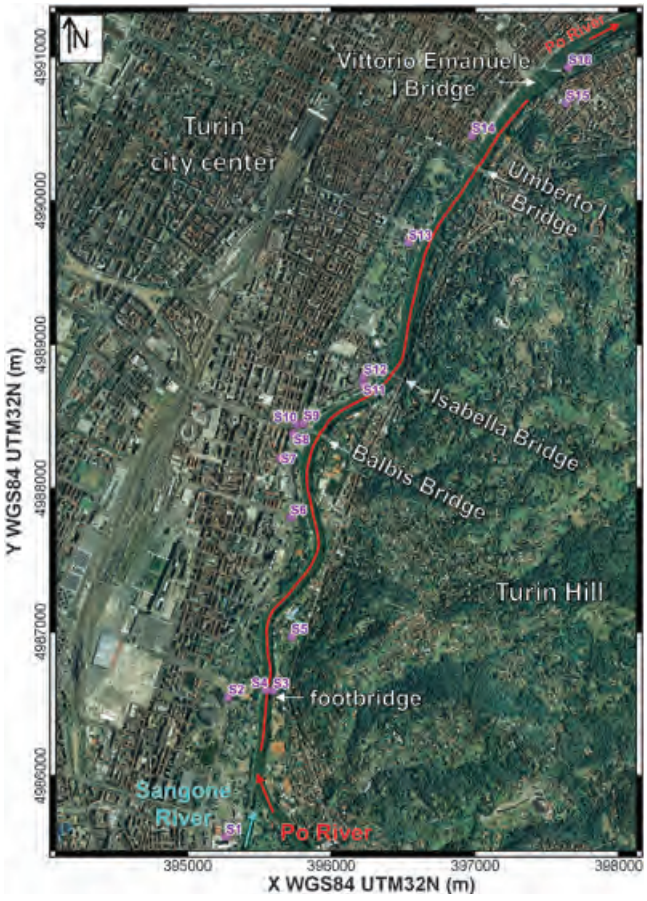

Figure 3. Detail of the investigated stretch (red line) of the Po river with the position of available stratigraphic information from the ARPA database (magenta) and evidence of crossing bridges.

DATA ACQUISITION

The GPR and CVES surveys were simultaneously performed on 7 May 2015. Acquisitions were conducted upstream and down-

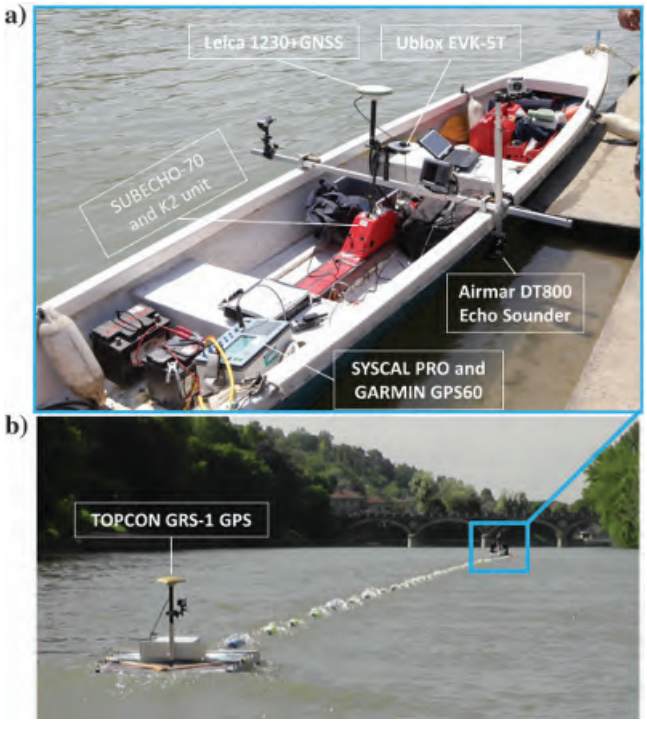

Figure 4. Instrumentation used during data acquisition on: (a) the main boat and (b) the raft at the end of the electric cable.

DOI:10.1190/geo2017-0071.1

stream of the river flow, for a total length of approximately 10 km (Figure 3). In this paper, the analysis is mainly focused on the downstream data sets.

The GPR survey was carried out in zero-offset reflection profiling mode, using a SUBECHO-70 monostatic antenna, with a peak frequency in air at 89 MHz, placed at the bottom of a fiber-reinforced plastic boat. The instrument for the acquisition of GPR data was a K2 IDS control unit. GPR data were sampled at 1.28 GHz for an 800 ns trace length. The average spatial sampling rate was 8trace/m. Just above the center of the GPR antenna, a global positioning system (GPS) device (ublox EVK-5T) was placed and directly connected to the K2 unit (Figure 4a). An independent GPS device (Leica 1230 + global navigation satellite systems [GNSS]) was additionally installed on the same boat (Figure 4a) for further processing.

The CVES survey was carried out pulling by boat a floating array of nine electrodes (total length of 96 m; Figure 4b). With the attention of leaving the electrodes below the water surface, the towed cable was equipped with plastic floaters and kept stretched by the friction with water of these elements and an additional small raft fixed at the end of the cable (Figure 4b). The adopted array had two current electrodes, in the cable part closest to the boat, followed by eight potential electrodes. The current electrodes (A and B) were 32 m spaced, whereas the potential dipoles had exponentially (integer power of two) increasing intervals (M1–M2: 0.5 m; M2–M3: 1 m; M3–M4: 2 m; M4–M5: 4 m; M5–M6: 8 m; M6–M7: 16 m; M7–M8: 32 m; see also Figure 5). Considering the length of the connection cable between the first current electrode and the boat, this configuration reached an overall length of approximately 105 m. Acquisitions were performed with a multichannel georesistivimeter (SYSCAL PRO in Sysmar upgrade — IRIS Instruments; Figure 4a), able to simultaneously acquire all the seven potential measurements. The georesistivimeter was connected to a GPS device (Garmin GPS60) and to a 170 kHz Airmar DT800 echo sounder (Figure 4a), located on the main boat, to have space and time information to control the acquisitions and create properly structured files. Each resistivity measurement was consequently coupled with the corresponding spatial position (on the boat) and with the bathymetry given by the echo sounder. The average spatial sampling interval between two consecutive resistivity and bathymetry measurements was 4 m. Besides the GARMIN GPS60, another GPS receiver was placed on the raft (Figure 4b), to recover information on the cable direction and to allow for correct positioning of the seven resistivity measurements along the cable length.

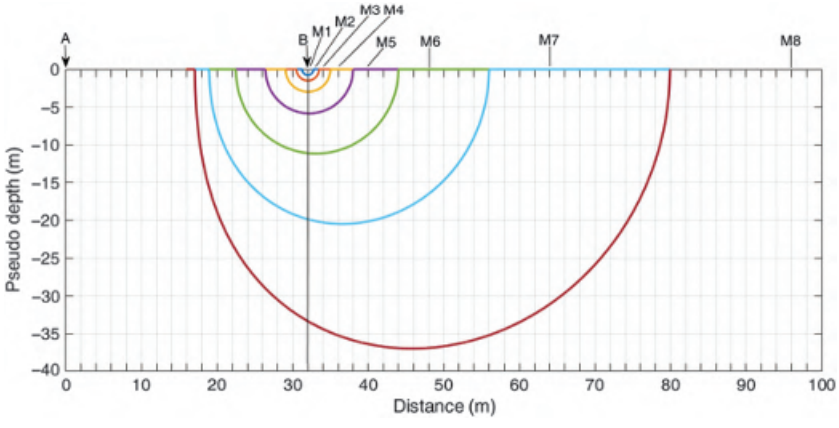

Figure 5. Equipotential lines from the middle of injecting and measuring dipoles and reference positioning under electrode B.

GEOREFERENCING ISSUES

The simultaneous execution of CVES, GPR, and echo sounder measurements along the river stretch, and the use of several GPS devices for each instrument, implied careful planning of the operations and required adequate georeferencing of all the acquired data for cross checking.

GPR-data georeferencing was made thanks to the external GPS device (ublox EVK-5T, Figure 4a) directly connected to the radar data logger, and no postprocessing operations were undertaken (Dabove and Manzino, 2017).

Conversely, CVES-survey positioning greatly differs from GPR, as far as the survey tracking is concerned. The investigated volume that significantly influences the measured resistivity depends on the measuring dipole and resistivity distribution (see Figure 5). The maximum influencing volume has an extension of the order of tens of meters in the transverse plane with respect to the cable axis, whereas the longitudinal extension is comparable with the cable length. As a consequence, differently from GPR acquisitions, CVES data cannot be treated as a point-like measurement. Furthermore, the cable-position tracking is fundamental when the array is not properly stretched during the survey and for the accurate positioning of detected localized anomalies.

The horizontal location along the cable of each CVES measurement was referred to as the position of the second current electrode (B in Figure 5). Under this electrode, the equipotential lines from the middle of the measuring dipoles reach the maximum depth for almost all the dipoles. Potential data at each dipole are consequently related to progressively increasing depths. The accurate position of the measurements along the survey implies, therefore, a correct georeferencing of the electrode B.

To estimate the correct direction and position of the cable two different GNSS instruments were used: a dual-frequency multiconstellation (GPS and GLONASS) receiver (Leica 1230 + GNSS, Figure 4a) on the main boat, and a single-frequency cartographic receiver (Topcon GRS-1, Figure 4b) on the raft. Coupled with these two receivers, two geodetic antennas were used: Leica LEIAX1230 + GNSS for the main boat and Topcon TPSPG-A1 for the raft. The use of dual constellation instruments guaranteed the positioning with a time interval of 0.5 s with a high level of accuracy.

The real-time and postprocessing approaches were followed. The position of the boat was determined in real-time using the Regione Piemonte CORSs (Continuous Operating Reference Stations, 2016) network, performing a network real-time kinematic positioning with the virtual reference station correction.

This approach provided an accuracy of the solutions approximately 2−4 cm for the main boat. Concerning the raft, raw data were postprocessed in a single base solution, considering as reference the Turin CORS (Dabove et al., 2016). This method allows to exploit the available capabilities for modern GNSS instruments. A subcentimeter accuracy was achieved considering only positions with fixed phase ambiguities

(Dabove and Manzino, 2017) and processing the data with Leica Geo Office v.8.4 software (provided by Leica Geosystems). The positions of the two receivers were recorded every second.

In Figure 6, an example of the tracking of the cable position is reported, for the survey area near the Isabella Bridge. With the adopted strategy for GNSS data elaboration, it was possible to correctly locate electrode B along the whole survey.

GEOPHYSICAL DATA PROCESSING

The GPR profiles were processed with the software Reflexw. For each profile, the processing steps included the following: dewow the traces to remove the very low-frequency trend; 400 ns time cut (because beyond this time, the recorded signals presented only noise); move the start time in correspondence to the main bang to obtain the correct traveltime; background removal (subtracting average) to attenuate the horizontal clutter along each profile (spatial high pass); and data filtering with a four-pole Butterworth band pass from 25 to 225 MHz. These operations succeeded in attenuating the low- and high-frequency noises. Subsequently, a divergence compensation was applied to recover the amplitude attenuation due to the geometric spreading. Furthermore, the frequency spectra were equalized with spectral whitening from 25 to 225 MHz, to obtain shorter reflected pulses. To enhance the continuity of the reflectors, a horizontal running average greater than 15 traces, roughly corresponding to a low-pass filter cutting wavelengths shorter than 2 m, was applied for smoothing the high-frequency spatial variations. Finally, after picking the bottom reflections, traces were muted above the picked times. An example of raw and processed radargrams are shown in Figure 7a and 7b for the upstream profile, from the acquisition start to 700 m distance.

Along the 5 km CVES survey, approximately 1200 readings were collected at each potential dipole, meaning an average of one VES every 4 m. A preliminary filtering was adopted to remove outliers, occasionally caused by defective water-electrode coupling. Figure 8 shows filtered apparent resistivities at the seven dipoles for the downstream data set and a statistical analysis of the data.

For both filtered data sets (upstream and downstream), the first three potential dipoles (at 0.5, 1, and 2 m spacing — see also Figure 5) substantially investigated the river water, which showed a relatively constant resistivity (average value of 43 Ωm — Figure 8) along the whole surveyed stretch. Along the survey, the retrieved depth of the riverbed varied from 2 to 10 m, with a mean depth approximately 5 m, thus confirming that the first three dipole measurements can be attributed to the water layer. Conversely, the following four dipoles showed higher variability (Figure 8), providing resistivity information about the riverbed sediments. This variation is more evident in the second part of the profile, from approximately 2500 m distance in Figure 8a. A remarkable anomaly is also evidenced in the last dipoles, at a distance of 450 m from the survey start. In addition, in the first and second parts of the profile, the seventh-dipole resistivities are frequently lower than the ones of the sixth dipole (Figure 8a). This evidence suggests the influence of a more conductive layer on the last-dipole measurements, located below the shallower riverbed sediments.

After preliminary data processing, CVES-data inversion was carried out following two different strategies: LCI and classical 2D tomographic approaches (ERT). These inversion techniques are based on different theoretical assumptions and algorithms. The LCI method for CVES-data inversion was first developed by Auken and Christiansen (2004). This approach is useful in the presence

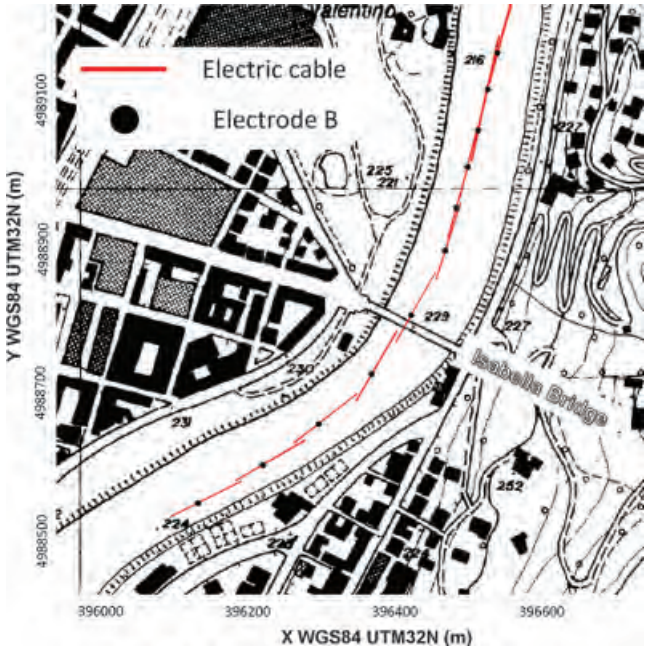

Figure 6. Example tracking of the cable position (red line) and electrode B (black dot) near the Isabella Bridge; reported positions are undersampled with respect to the real data acquisition.

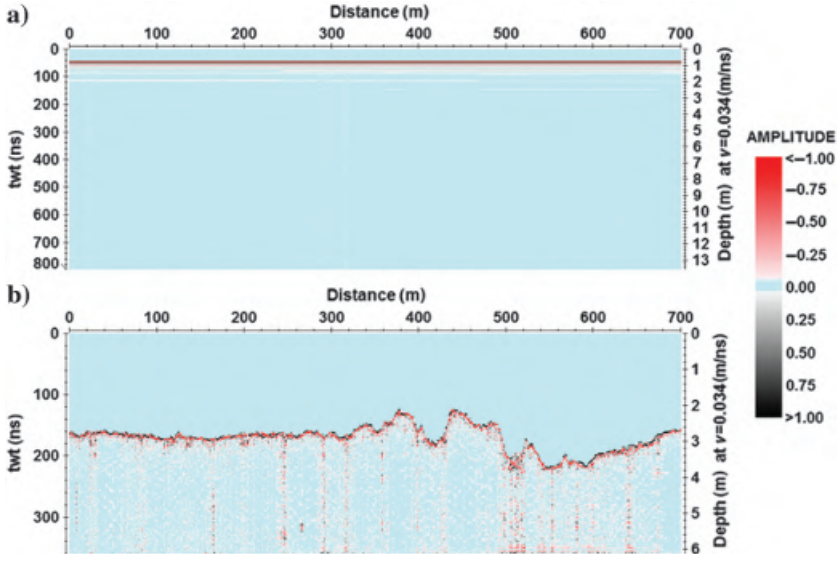

Figure 7. (a) Raw and (b) processed radargrams for the upstream profile from the beginning of the acquisitions to a distance of 700 m.

DOI:10.1190/geo2017-0071.1

of a predominantly layered subsurface (a typical sedimentary environment) because it considers a pseudo-2D layered parameterization of the investigated medium. The inversion is based on an algorithm formulated for 1D inversion, implemented with the introduction of lateral constraints on resistivities, depths (primary parameters), and thicknesses (secondary parameter) between subsequent VES. These constraints allow for exploiting the available a priori information and for transmitting their influence throughout the profile. The inversion result is a set of 1D consecutive resistivity models, each one corresponding to a sounding, composing a pseudo 2D section. Each 1D model consists of a limited number of layers characterized by a resistivity and a thickness value. The LCI approach adopted in this work is similar to the one already presented by Sambuelli et al. (2011) and Colombero et al. (2014), where the inversion methodology is described in greater detail. Before inverting CVES data with the LCI approach, to establish a correct depth parameterization, it is advised to assign to the measurements an apparent investigation depth. Considering the used dipole-dipole configuration, these apparent depths were conventionally chosen as the intersections between the equipotential lines corresponding to the midpoint of each potential dipole and the vertical direction beneath the second current electrode (B, in Figure 5). The chosen parameterization for the LCI was a three-layer model. The first layer represents the water column, the second one represents the alluvial deposits, and the third layer corresponds to the Turin-Hill marls, which are attended at depth. Given the lateral variability of the acquired data (Figure 8), the constraints controlling the lateral homogeneity of the model are key parameters for the inversion. As a consequence, the strength of the constraints is chosen taking into account the attended geologic setting. Particularly, a strong constraint is applied if the expected lateral variability is small; whereas constraints are weaker in the case of large lateral variations (Colombero et al., 2014). Because the contemporary acquisition of GPR, CVES, and echo-sounder data provided the bathymetry and the water average resistivity value, the water-column parameters were substantially a priori known for the CVES inversion. The first-layer thickness was therefore fixed, and its resistivity was kept constant (43 Ωm) along the profile length. No constraints were set for the second layer resistivity, whereas the resistivity of the third layer was set in the range 23 ± 20 Ωm (from a preliminary inversion of the data), with the aim of forcing the inversion to find a lateral continuity for the deepest conductive deposits.

As a comparison, the same data set was additionally processed following a classical 2D tomographic inversion approach, using Res2DInv software (Geotomo Software). This 2D inversion algorithm is based on the smoothness-constrained least-squares method (deGroot-Hedlin and Constable, 1990; Sasaki et al., 1992). Also, for this inversion approach, strong a priori constraints were imposed for depth and resistivity of the water layer. This could be achieved using a distorted finite-element grid to calculate the apparent resistivity values for the inversion model; in this way, the nodes along the bottom row of the water mesh are adjusted to make the waterbody geometry match with bathymetry data (Loke and Lane, 2004). In this way, the inversion software only determined the resistivity values in the lower part of the model, to accurately reproduce the observed resistivity measurements. An initial and a minimum damping factor of 0.16 and 0.015 were set. An increase of 1.05 with depth was chosen for the damping factor, and the software function for the related optimization was used. Concerning the flatness filters, the vertical/horizontal flatness filter ratio was fixed to 0.75, to force the program to find the lateral continuity of the layers, without compromising the definition of vertically elongated forms. No smoothness constraints were applied during the inversion process.

RESULTS

In Figure 9, the processed radargrams along the whole investigated stretch are reported. With the GPR survey, an accurate imaging of the bed forms was obtained. Throughout the survey, GPR pulse did not penetrate the bottom sediments; therefore, no extended information on the bedding could be retrieved.

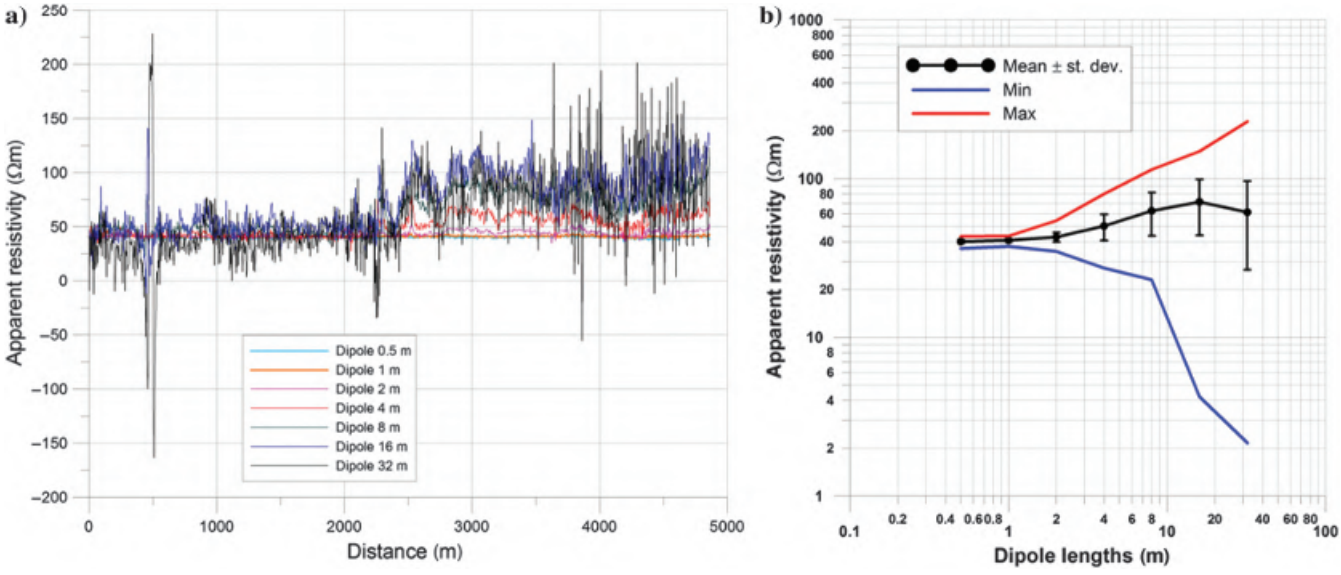

Figure 8. Apparent resistivities measured at each dipole along the downstream data set after filtering: (a) the whole data along the survey length and (b) the statistical analysis.

In Figure 9a, the processed radargram for the first 400 m of the downstream profile is presented. A series of quite regular waving shapes are observed from left to right (flow direction). The same morphologies continue downstream (Figure 9b and 9c), until the distance of 2240 m (Figure 9d), where the form with two symmetrical reliefs that precede and follow a depression corresponds to the Balbis Bridge. No waving bed forms can be found downstream of Balbis Bridge as can be seen in the following panels of Figure 9e–9h. Depressions partially similar to the ones observed at the Balbis Bridge are also visible near the other bridges, as evidenced in Figure 9e and 9h. These can be related to the increase in river flow velocities due to the obstruction of the bridge piers, which result in a local excavation of the river bottom and a consequent potential scour of the piers.

Given the variability of water depths along the stretch (from 2 to 10 m), not always was the radar signal able to penetrate the water column and obtain a reflection from the bottom sediments. This can be observed near the progressive 1050 and 1650 m (Figure 9b and 9c), where indeed the higher water depths are retrieved from the echo sounder survey (see later Figure 10 in the same locations). The variability in water depths within the investigated stretch can be mainly related to lateral streams and channels transversally cutting the river flow and locally eroding the bottom.

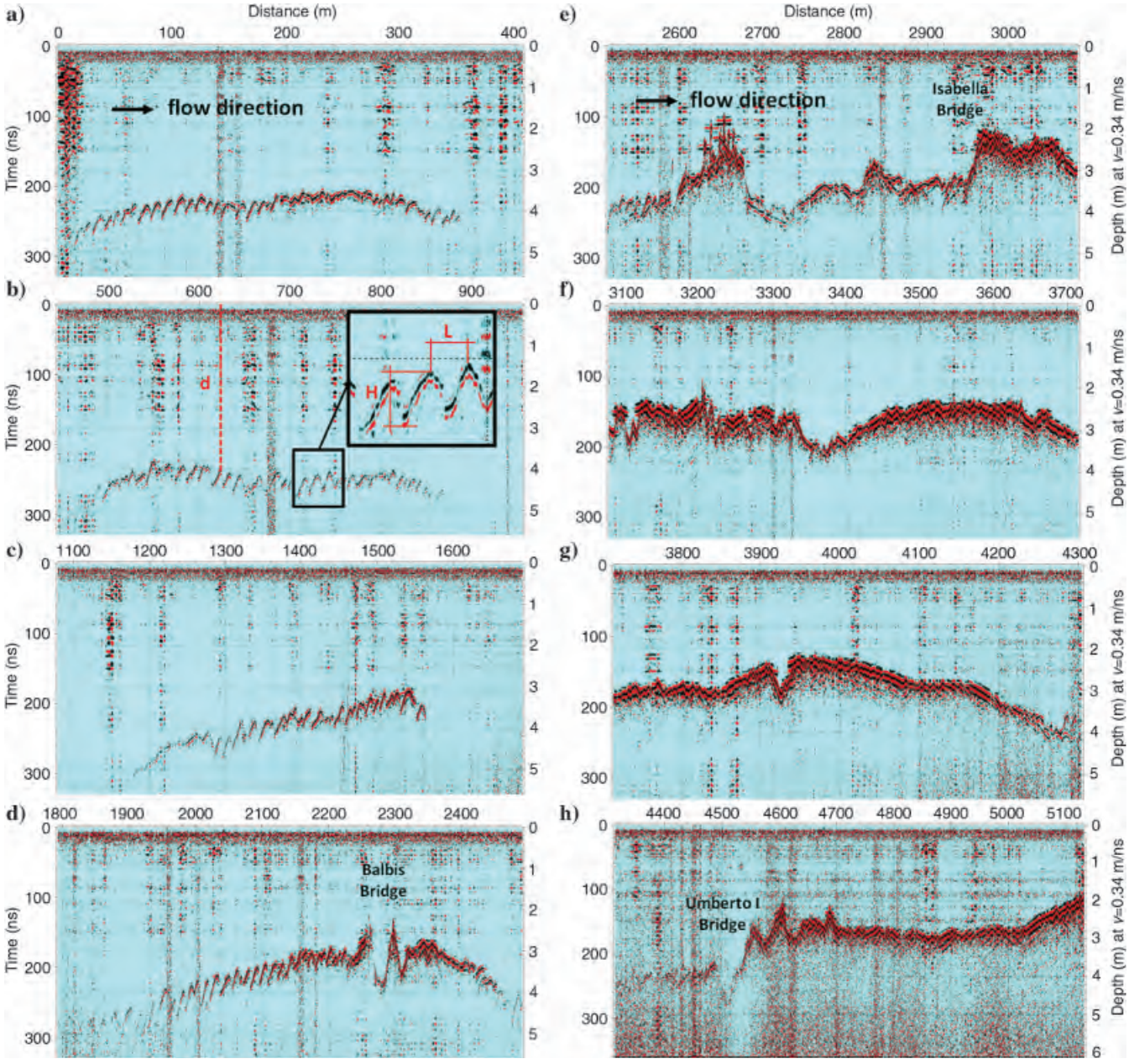

Figure 9. Processed radargrams for the downstream survey: (a-h) for an increasing distance from the beginning of the downstream profile (vertical exaggeration approximately 25×); (b) parameters for the determination of dunes shapes are also reported: dune height H (m), dune wavelength L (m), and water depth above the dune d (m).

DOI:10.1190/geo2017-0071.1

In Figure 10, the results of the inversions of the CVES data from the downstream data set, for the LCI and for the 2D tomography approaches, are reported. To maintain a readable vertical scale, the whole investigated stretch has been split into 1 km profiles. Available stratigraphic data from ARPA database, consisting of logs and water wells in the surroundings of the river banks (Figure 3), are overlapped to the inversion results.

LCI and tomographic results are highly coherent along the investigated stretch. Below the water layer (blanked in all sections), a thick layer of sediments with resistivity higher than the water (>43 Ωm) is observed. The thickness of this layer is not laterally homogeneous and progressively increases toward the north (from a few meters to more than 15 m), also showing irregular depressions and reliefs at its bottom. The resistivity of this layer ranges from 45 up to 250 Ωm. The lowest values are observed in the first 2400 m of the survey (43–90 Ωm), until Balbis Bridge; from this point to the end of the survey, the resistivity increase (mean value of approximately 150 Ω). The bottom part of all sections is characterized by sediments with resistivity (20–40 Ωm) lower than water resistivity.

A strong electrical anomaly, already noticeable in the raw data (Figure 8) is also observed near the first bridge of the survey (footbridge, 460 m), due to the pier foundation structure. These data were removed from the computation with the LCI approach, but they remained in the 2D tomographic results (Figure 10a). It should be underlined that the correct positioning and interpretation of this anomaly was possible only with the accurate georeferencing of GPS data.

DISCUSSION

Because the GPR signal did not penetrate below the riverbed, the only possibility to argue sediment characteristics from the GPR survey was related to the peculiar riverbed morphology observed in the first part of the downstream profile (Figure 9). This morphology can be preliminary attributed to the presence of subaqueous sand dunes. The presence of these dunes only in the first part of the profile suggests a variation in sediment properties after Balbis Bridge. Few available stratigraphic logs (from S3, S4, and S7 to S11, S12, and S15) seem to confirm this change in the bottom-sediment nature; from a prevalent silty and sandy composition in the south, to the dominant presence of gravels toward the north. Another partial confirmation of the different grain-size distributions is the less marked erosion near bridge piers in the second part of the profile with respect to the one evidenced at the Balbis Bridge location.

To validate this hypothesis, 31 clear dune shapes were selected for the measurement of meaningful related geometric features (Figure 9b). The considered parameters were the following: dune height H (m), dune wavelength L (m), and water depth above the dune d (m) (Figure 11).

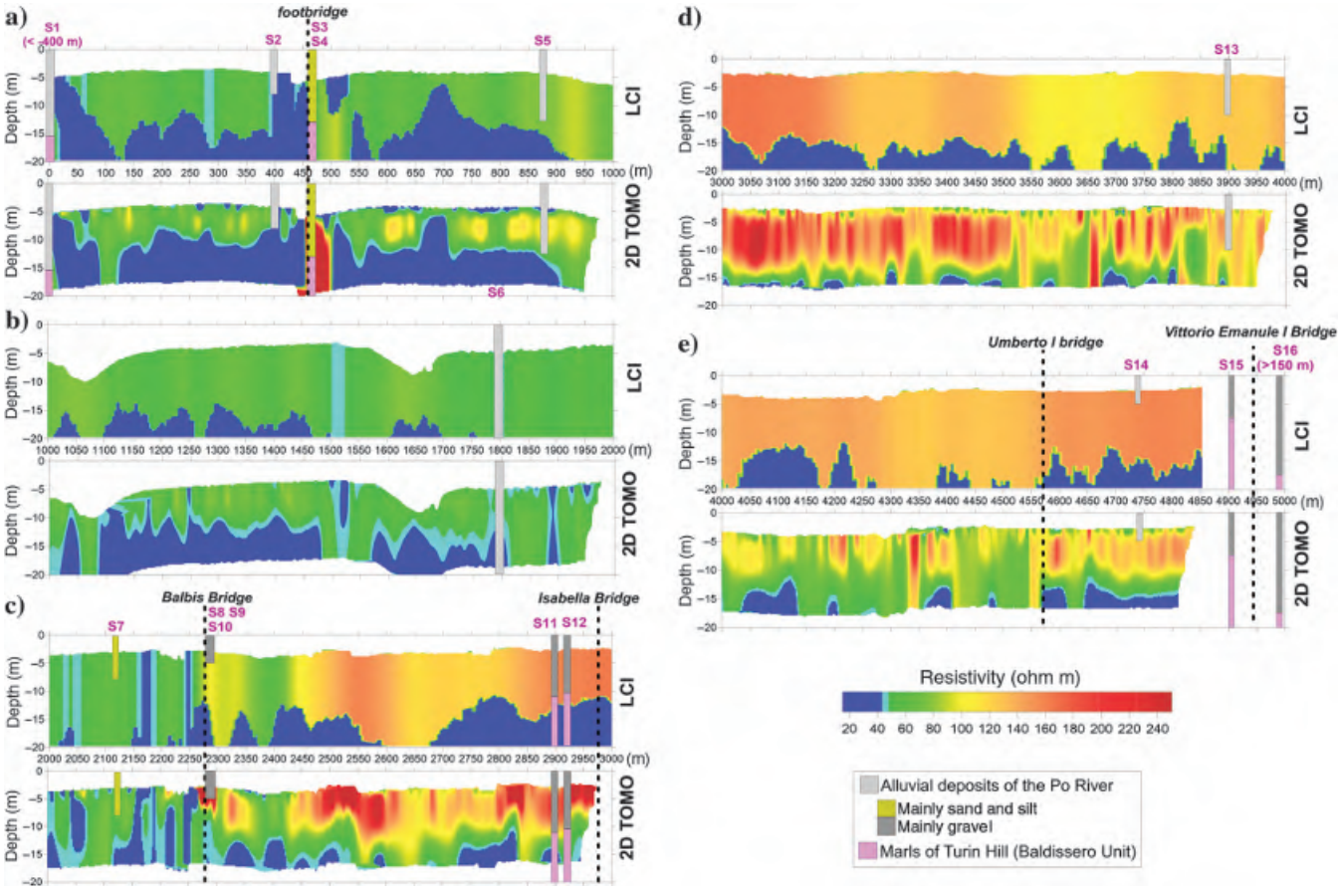

Figure 10. Inversion of CVES data: (a-e) the results of (top) LCI and (bottom) 2D tomography are reported in consecutive segments of 1000 m (vertical exaggeration approximately 10×).

Within the wide literature on river-sediment forms, reference was made to the work of Flemming (2000), in which published data related to natural flows and experimental flume systems were collected. Diagrams relating the geometric parameters H, L, and d to the grain size of constituting deposits were retrieved. The results obtained in the present case study are overlapped to these diagrams in Figure 12.

Particularly, retrieved parameters are consistent with the measurements of other authors (Keller and Richards, 1967; Terwindt, 1971; Ozasa, 1974; Werner et al., 1974; Jackson, 1976; Flemming, 1978; Rubin and McCulloch, 1980) on river subaqueous sand dunes on the L-d plane (Figure 12a) and on the H-d plane (Figure 12b), where they are compatible with the boundaries given by Allen (1968). In addition, the overlay of the present data on the L-H diagram (Figure 12c) confirms the silt and fine sands to be likely the dominant grain sizes for the shallower riverbed in the first part of the downstream profile, until Balbis Bridge.

The first layer of sediments imaged in the resistivity sections can be therefore related to the presence of fluvial deposits (mainly silt, sands, and gravels) of the Po River. The increase in resistivity from south to north can be linked either to a local increase in the sediment grain size or to the presence of more compacted or cemented horizons. This variation in the grain size is coherent with GPR bed forms and locally available stratigraphic information. These last report shallow silty and sandy alluvial deposits before Balbis Bridge (i.e., S3, S4, and S7), whereas gravelly deposits are detected thereafter (i.e., S8, S11-12, and S15). Downstream of Balbis Bridge, the river bottom was also historically recognized as constituted by gravel and pebbles. Two bars with vegetation are indeed reported in XIX-century documents (Figure 13).

In general, water and its chemistry are crucial aspects in the imaging of the subsurface with geoelectric methods. Waterborne methods have the advantage that the water-column parameters can be reliably extracted from measured data (first three potential dipoles in Figure 8). Independent water samples were however acquired, in

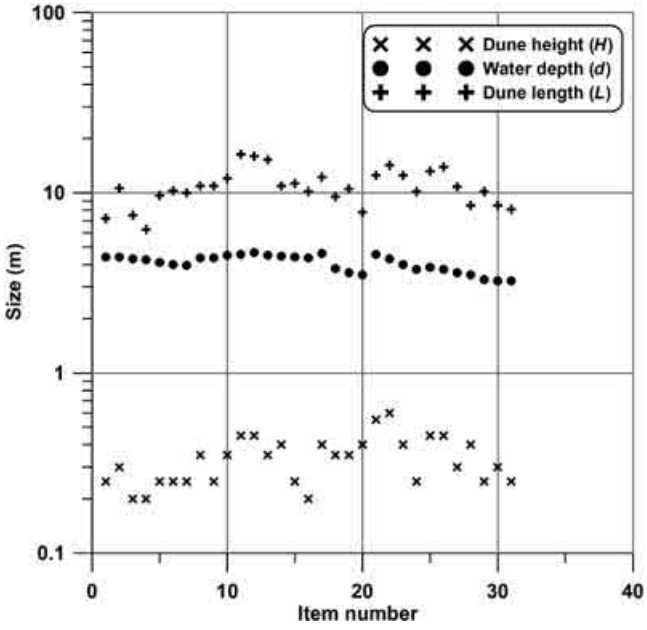

Figure 11. Sand dunes shape parameters from the GPR survey.

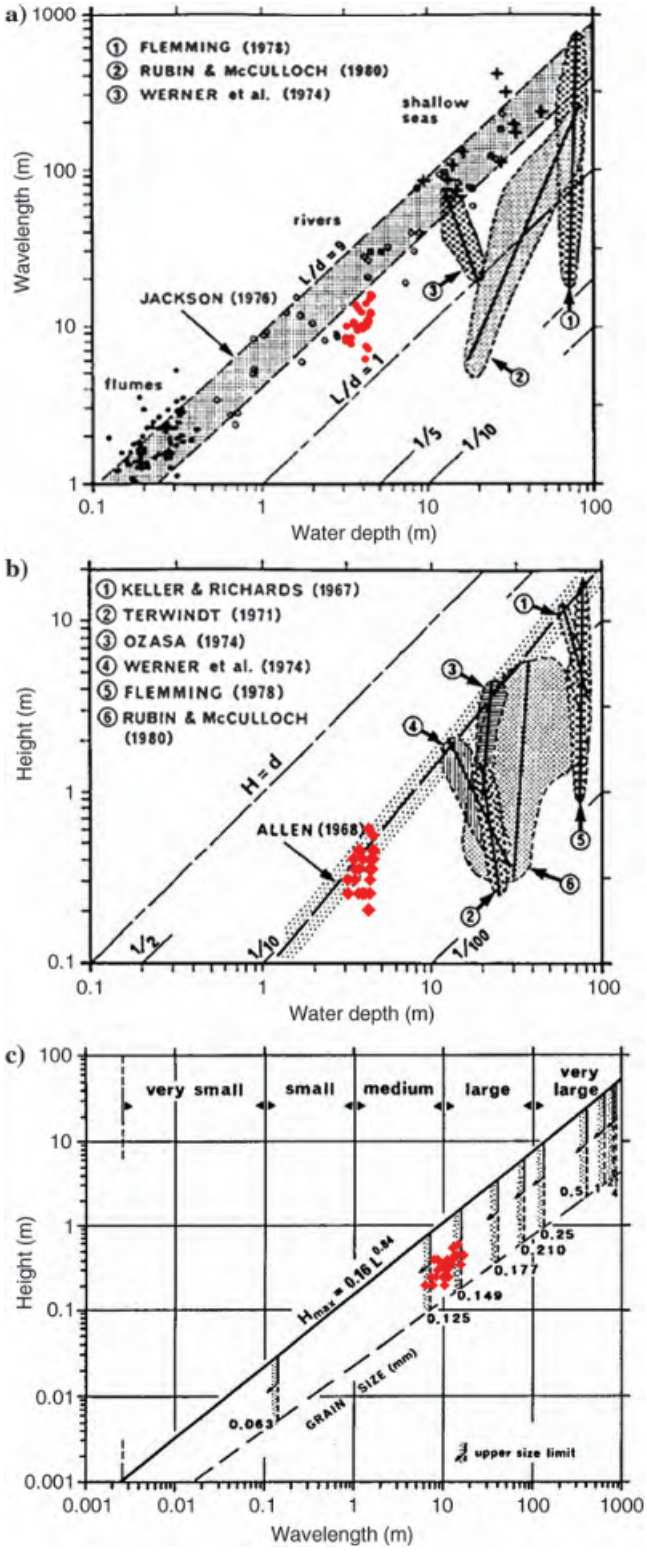

Figure 12. Comparison of sand dunes shape parameters of our study with the ones reported in Flemming (2000) on (a) L-d plane, (b) H-d plane, and (c) H-L plane with correlation with grain size (modified from Fleming, 2000).

a date proximal to the geophysical surveys (i.e., 17 June 2015), to be later tested for chemical content. The water under examination was a Ca-HCO_3 type water with fairly constant values along the river stretch (Pascal, 2015). Similar water properties are also recognized for the water table (Regione Piemonte database, 2017), confirming the drainage effect of the river.

LCI and tomographic results are highly comparable particularly in the first 2400 m of the profile, in which a more homogeneous river bottom configuration is expected. Due to the three-layer model assumption, and to the pseudo 2D nature of the interpretation, LCI results report a unique mean value for the shallowest sediments. In addition, LCI results are laterally smoother due to the adopted later constraints. Conversely, 2D tomography distinguishes localized higher resistivity anomalies within the shallowest sediments, which may better reflect locally compacted or coarser grain-size horizons (see the exemplificative comparisons in Figure 10a and 10c).

The lower resistivity at the bottom of both inverted sections can be likely related to the marls of Turin-Hill marine sequence. The morphology of this horizon is quite undulating, suggesting strong erosional phenomena along the main flow of the river and at the confluence of the lateral tributary streams. The presence of this deeper layer is evidenced in both the inversions. However, LCI depicts a more sharp and precise transition with respect to tomographic sections. As a result, the position of this horizon partially differs in the two interpretations. Unfortunately, the investigation depth of the available direct surveys did not always reach the marly deposits. Stratigraphic data and geophysical results are found to be in good agreement for the surveys with higher investigation depths. Particularly, stratigraphic information near the Isabella Bridge (Figure 10c), confirming the presence of the marls deposits at depth, appear to compare better with the LCI than with the tomography. As already underlined, LCI model configuration and adopted constraints were on purpose devised for the detection of this interface, in terms of depth and lateral geometry.

Figure 13. Map of Turin (1840) with evidence of the historically vegetated bars and actual and past bridges (modified from Sassi Perino and Faraggiana, 1995).

CONCLUSION

In this study, a fast and reliable reconstruction of the riverbed deposits was obtained along a 5 km stretch of the Po river, within the urban area of Turin, by means of waterborne GPR and CVES surveys. In the shallowest riverbed, alluvial deposits of the Po Plain were detected, with variable thickness along the investigated line and variable dominant grain size. Finer sediments (i.e., silt and sands) dominate upstream Balbis Bridge, as confirmed by CVES lower resistivity values, by the presence of sand dunes in the GPR sections and by available stratigraphic information. Coarser deposits (i.e., gravel and pebbles) are prevalent downstream Balbis Bridge, in agreement with the CVES higher resistivity results, the absence of bed forms in the radargrams, and the available historical information and stratigraphic logs. These shallower alluvial deposits directly lie on the marly deposits of the Turin Hill. The depth of this interface along the stretch was laterally reconstructed from CVES data and locally confirmed by stratigraphic logs. The morphology of the depicted interface is undulating, suggesting strong erosional phenomena along the main flow of the river and at the confluence of the lateral tributary streams. Downstream Balbis Bridge, the presence of a thin layer of fine sediments between the gravelly alluvial deposits and the Turin-Hill marls cannot be either confirmed or excluded due to the vertical resolution of the CVES survey and the absence of GPR information below the riverbed.

The presented case history confirms the effectiveness of waterborne surveys for geologic prospecting in water-covered and difficult-to-access areas. Waterborne methods can therefore be considered a valuable alternative for the investigation of wide submerged areas in a cost-effective way, enabling us to profitably extend local information coming from direct soundings.

ACKNOWLEDGMENTS

The authors would like to thank the municipality of Turin (Servizio Ponti, Vie d'acqua ed infrastructure, in particular, G. Marengo), the Cerea Royal Rowing Club for supplying boats and pilots, D. Franco, B. Horea, and P. Maschio for their support in data acquisition and survey documentation.

REFERENCES

Allen, D., and N. Merrick, 2007, Robust 1D inversion of large towed geoelectric array datasets used for hydrogeological studies: Exploration Geophysics, **38**, 50–59, doi: 10.1071/EG07003.
Allen, J. R. L., 1968, Current ripples: North-Holland Publishing Co., 433.
Annan, A. P., and J. L. Davis, 1977, Impulse radar applied to ice thickness measurements and freshwater bathymetry: Report of Activities. Part B: Geological Survey of Canada, 63–65, doi: 10.4095/102754.

Arcone, S. A., D. Finnegan, and G. Boitnott, 2010, GPR characterization of a lacustrine UXO site: Geophysics, **75**, no. 4, WA221–WA239, doi: 10.1190/1.3467782.

Arcone, S. A., D. Finnegan, and J. E. Laatsch, 2006, Bathymetric and subbottom surveying in shallow and conductive water: Proceedings of the 11th International Conference on Ground Penetrating Radar on CDROM.

Arpa Piemonte, 2016, http://webgis.arpa.piemonte.it, accessed 14 December 2016.

Auken, E., and A. V. Christiansen, 2004, Layered and laterally constrained 2D inversion of resistivity data: Geophysics, **69**, 752–761, doi: 10.1190/1.1759461.

Befus, K. M., M. B. Cardenas, J. B. Ong, and V. A. Zlotnik, 2012, Classification and delineation of groundwater-lake interactions in the Nebraska Sand Hills (USA) using electrical resistivity patterns: Hydrogeology Journal, **20**, 1483–1495, doi: 10.1007/s10040-012-0891-x.

Boano, P., M. G. Forno, and S. Lucchesi, 2004, Pleistocene deformation of the Collina di Torino inferred from the modelling of their fluvial succession: II Quaternario, **17**, 145–150.

Bortolami, G. C., G. C. Crema, R. Malaroda, F. Petrucci, R. Sacchi, C. Sturani, and S. Venzo, 1969, Foglio 56 'Torino' della Carta Geologica d'Italia alla scala 1:1000.000, IIa ed.: Servizio Geologico d'Italia.

Bove, A., D. Casaccio, E. Destefanis, D. A. De Luca, M. Lasagna, L. Masciocco, L. Ossella, and M. Tonussi, 2005, Piezometria della falda superficiale nel territorio di pianura della Regione Piemonte: Idrogeologia della Regione Piemonte, Regione Piemonte, Direzione Pianificazione Risorse Idriche, CD-ROM, articolo II, 10 (in Italian).

Bradbury, K. R., and R. W. Taylor, 1984, Determination of the hydrogeological properties of lakebeds using offshore geophysical surveys: Ground Water, **22**, 690–695, doi: 10.1111/j.1745-6584.1984.tb01437.

Butler, K. E., 2009, Trends in waterborne electrical and EM induction methods for high resolution sub-bottom imaging: Near Surface Geophysics, **7**, 241–246.

Castellarin, A., 1994, Strutturazione eo: e mesoalpina dell'Appennino settentrionale attorno al nodo ligure: Studi Geologici Camerti, special volume CROP 1-1, 99–108 (in Italian).

Civita, M., and S. Pizzo, 2001, L'evoluzione spazio-temporale del livello piezometrico dell'acquifero libero nel sottosuolo di Torino: GEAM, 271–287 (in Italian).

Colombero, C., C. Comina, F. Gianotti, and L. Sambuelli, 2014, Waterborne and on-land electrical surveys to suggest the geological evolution of a glacial lake in NW Italy: Journal of Applied Geophysics, **105**, 191–202, doi: 10.1016/j.jappgeo.2014.03.020.

CORSs (Continuous Operating Reference Stations) network, 2016, http://www.spingnss.it/spiderweb/frmIndex.aspx, accessed 14 December 2016.

Dabove, P., A. Cina, and A. M. Manzino, 2016, How reliable is a Virtual RINEX?: 2016 IEEE/ION Position, Location and Navigation Symposium (PLANS), 255–262.

Dabove, P., and A. M. Manzino, 2017, Artificial neural network for detecting incorrectly fixed phase ambiguities for L1 mass-market receivers: GPS Solutions, **21**, 1213–1219.

deGroot-Hedlin, C., and S. Constable, 1990, Occam's inversion to generate smooth, two dimensional models form magnetotelluric data. Geophysics, **55**, 1613–1624, doi: 10.1190/1.1442813.

Dela Pierre, F., P. Clari, E. Bernardi, M. Natalicchio, E. Costa, S. Cavagna, F. Lozar, S. Lugli, V. Manzi, M. Roveri, and D. Violanti, 2012, Messinian carbonate-rich beds of the Tertiary Piedmont Basin (NW Italy): Microbially-mediated products straddling the onset of the salinity crisis: Palaeogeography, Palaeoclimatology, Palaeoecology, **344-345**, 78–93, doi: 10.1016/j.palaeo.2012.05.022.

Festa, A., P. Boano, A. Irace, S. Lucchesi, M. G. Forno, F. Dela Pierre, and F. Piana, 2009, Foglio 156 'Torino Est' della Carta Geologica d'Italia alla scala 1:50.000: APAT, Agenzia per la Protezione dell'Ambiente e per i Servizi Tecnici- Dipartimento Difesa del Suolo, Roma.

Flemming, B. W., 1978, Underwater sand dunes along the southeast African continental margin — Observations and implications: Marine Geology, **26**, 177–198, doi: 10.1016/0025-3227(78)90059-2.

Flemming, B. W., 2000, The role of grain size, water depth and flow velocity as scaling factors controlling the size of subaqueous dunes, in A. Trentesaux, and T. Garlan, eds., Proceedings of the Marine Sandwave Dynamics, 23–24 March 2000: University of Lille, 55–60.

Forno, M. G., G. Ben, P. Boano, V. Boero, and R. Compagnoni, 2002, Lembi di depositi fluviali provenienti dai bacini alpini nordoccidentali sulla Collina di Torino presso Villa Gualino (NW Italy): II Quaternario, **15**, 175–185 (in Italian).

Forno, M. G., and S. Lucchesi, 2005, La successione fluviale terrazzata pleistocenica dei versanti occidentale e nordoccidentale della Collina di Torino: II Quaternario, **18**, 123–134 (in Italian).

Forno, M. G., and S. Lucchesi, 2015, Relicts of the Pleistocene Po Plain on the Western and Southern slopes of Turin Hill (NW Italy): Journal of Maps, **12**, 394–406, doi: 10.1080/17445647.2015.1027481.

Jackson, R. G., 1976, Sedimentological and fluid dynamic implications of the turbulent bursting phenomenon in geophysical flows: Journal of Fluid Mechanics, **77**, 531–560, doi: 10.1017/S0022112076002243.

Keller, G. H., and A. F. Richards, 1967, Sediments of the Malacca Strait, Southeast Asia: Journal of Sedimentary Petrology, **37**, 102–127.

Lin, Y. T., C. H. Wu, D. Fratta, and K. J. S. Kung, 2010, An integrated acoustic and electromagnetic wave-based technique to estimate subbottom sediments properties in a freshwater environment: Near Surface Geophysics, **8**, 213–221, doi: 10.3997/1873-0604.2010006.

Loke, M. H., and J. W. Lane, 2004, Inversion of data from electrical resistivity imaging surveys in water-covered areas: Exploration Geophysics, **35**, 266–271, doi: 10.1071/EG04266.

Lollino, G., P. Faliero, and M. Rosso, 2000, Metodologiea radioisotopiche per la determinazione dei parametri idrogeologici della radioattività naturale presso il campo sperimentale del CNR-IRPI di Torino, Geoingegneria Ambientale e Mineraria: GEAM, **100**, 149–153 (in Italian).

Mitchell, N., J. E. Nyquist, L. Toran, D. O. Rosenberry, and J. S. Mikochik, 2008, Electrical resistivity as a tool for identifying geologic heterogeneities which control seepage at Mirror Lake, NH: Proceedings of the SAGEEP 2008, CDrom, 749–759.

Mosca, P., 2006, Neogene basin evolution in the Western Po Plain (NW Italy): Insights from seismic interpretations, subsidence analysis and low (U-Th)/He thermochronology: Ph.D. thesis, Vrije University.

Ozasa, H., 1974, Field investigations of large submarine sand waves: Coastal Engineering in Japan, **17**, 155–184.

Pascal, I., 2015, Geophysical and geochemical survey on the southern stretch of the Po River in Turin: Master thesis, Politecnico di Torino.

Regione Piemonte database, 2017, http://www.regione.piemonte.it/monitgis/jsp/cartografia, accessed 21 June 2017.

Rubin, D. M., and D. S. McCulloch, 1980, Single and superimposed bed forms: A synthesis of San Francisco Bay and flume observations: Sedimentary Geology, **26**, 207–231, doi: 10.1016/0037-0738(80)90012-3.

Rucker, D. F., G. E. Noonan, and W. J. Greenwood, 2011, Electrical resistivity in support of geological mapping along the Panama: Canal Engineering Geology, **117**, 121–133, doi: 10.1016/j.enggeo.2010.10.012.

Sambuelli, L., and S. Bava, 2011, Case study: A GPR survey on a Morainic lake in northern Italy for bathymetry, water volume and sediment characterization: Journal of Applied Geophysics, **81**, 48–56, doi: 10.1016/j.jappgeo.2011.09.016.

Sambuelli, L., and K. E. Butler, 2009, Foreword: Special issue on high resolution geophysics for shallow water: Near Surface Geophysics, **7**, 3–4.

Sambuelli, L., C. Calzoni, and M. Pesenti, 2009, Waterborne GPR survey for estimating bottom-sediment variability: A survey on the Po River, Turin, Italy: Geophysics, **74**, no. 4, B95–B102, doi: 10.1190/1.3119262.

Sambuelli, L., C. Comina, S. Bava, and C. Piatti, 2011, Magnetic, electrical, and GPR waterborne surveys of moraine deposits beneath a lake: A case history from Turin, Italy: Geophysics, **76**, no. 6, B213–B224, doi: 10.1190/geo2011-0053.1.

Sangiovanni, C., 2017, Studio idrogeologico del settore sud orientale della pianura torinese: Master thesis, Università degli Studi di Torino.

Sasaki, Y., Y. Yoneda, and K. Matsuo, 1992, Resistivity imaging of controlled-source audio frequency magnetotelluric data: Geophysics, **57**, 952–955, doi: 10.1190/1.1443309.

Sassi Perino, A., and G. Faraggiana, 1995, I trentasei ponti di Torino: Edizioni del Capricorno.

Terwindt, J. H. J., 1971, Sand waves in the southern bight of the North Sea: Marine Geology, **10**, 51–67, doi: 10.1016/0025-3227(71)90076-4.

Werner, F., W. E. Arntz, and K. Tauchgruppe, 1974, Sedimentologie und Ökologie eines ruhenden Riesenrippelfeldes: Meyniana, **26**, 39–59.